Mechanically robust ANF/MXene composite films with tunable electromagnetic interference shielding performance

Chuanxin Weng[a,b], Tianle Xing[c], Hao Jin[a], Guorui Wang[d], Zhaohe Dai[e], Yongmao Pei[f], Luqi Liu[a,*], Zhong Zhang[a,*]

[a] CAS Key Laboratory of Nanosystem and Hierarchical Fabrication and CAS Center for Excellence in Nanoscience, National Center for Nanoscience and Technology, Beijing 100190, China
[b] University of Chinese Academy of Sciences, Beijing 100049, China
[c] School of Aeronautic Science and Engineering, Beihang University, Beijing 100191, China
[d] Department of Mechanical and Industrial Engineering, University of Toronto, Toronto, Ontario M5S 3G8, Canada
[e] Center for Mechanics of Solids, Structures and Materials, Department of Aerospace Engineering and Engineering Mechanics, The University of Texas at Austin, Austin, TX 78712, USA
[f] State Key Laboratory for Turbulence and Complex Systems, College of Engineering, Peking University, Beijing 100871, China

ARTICLE INFO

ABSTRACT

MXene-based materials have been widely studied recently for effective electromagnetic interference (EMI) shielding due to the prominent intrinsic electrical conductivity. Nevertheless, the poor mechanical performance of pure MXene films limits the practical application in EMI shielding. Thus, we integrate MXene with aramid nanofiber (ANF) to develop a composite film with layered structure through a simple vacuum-assisted filtration method. The resulting ANF/MXene (20/80) composite exhibits a high electrical conductivity of 879.0 S/cm, EMI shielding effectiveness (SE) of 40.6 dB and specific SE (SSE/t, SE divided by the density and thickness) of 50,491 dB·cm^2·g^{-1} with an ultrathin thickness of 3.2 μm. Furthermore, the ANF/MXene (60/40) realizes a balance between mechanical properties and EMI shielding performance with the strength of 201.3 MPa and SE of 28.1 dB, which enables the ANF/MXene composite films as promising EMI shielding materials with excellent mechanical robustness.

1. Introduction

Thin films with capabilities of electromagnetic interference (EMI) shielding have played an essential role in electronic device applications. Recently, the development of flexible and wearable electronics urges EMI shielding films from traditional metal foils to composite films including nanomaterials. Compared with traditional metal EMI shielding materials, various nanomaterials-based composite films (e.g., CNT [1–3], graphene [4–6], and metal nanowires [7–9]) have shown great advantages in terms of low density, easy processability, high electrical conductivity, excellent corrosion resistance, great flexibility, and so on. For instance, Zeng et al. fabricated lightweight and flexible multi-walled carbon nanotube/waterborne polyurethane (MWCNT/WPU) composite films with high MWCNT loading of 76 wt%, which showed superior EMI shielding effectiveness in the X-band (800 μm, 80 dB) [1]. Jia et al. reported that nacre-like reduced graphene oxide/calcium alginate (rGO/CA) composite films could show an EMI shielding

effectiveness of 25.7 dB once the thickness was reduced to 12 μm [6]. The EMI shielding performance of these composite films is comparable and even superior to traditional metal films.

For the composite films, the EMI shielding is usually achieved by the reflection, absorption, and multiple reflections of electromagnetic waves [10–13]. The electromagnetic waves are first reflected by the conductive surface of composite films, then the remaining electromagnetic waves would be attenuated by multiple reflection and absorption of conductive fillers. Thus, the polymer not only endows the composite with low density, easy processability, excellent corrosion resistance, and great flexibility but also facilitates the multiple internal reflections between conductive fillers, eventually resulting in absorption of electromagnetic waves and improvement of EMI shielding performance [1].

More recently, MXene, a new class of two-dimensional (2D) materials, consist of transition metal carbides, nitrides, or carbonitrides and thus feature both metallic conductivity of transition metal carbides and

---

hydrophilic properties [14–16]. Expectedly, the remarkable electrical conductivity and solution-compatible nature of MXene make them particularly suitable for EMI shielding applications [17–19]. Shahzad et al. first demonstrated the superior EMI shielding performance of neat MXene and sodium alginate-based MXene composite films [17]. However, the low mechanical strength of MXene films further hinders their practical application in EMI shielding. An effective way to improve the mechanical properties of MXene films is to incorporate with polymers to prepare composite materials. So far, significant progress has been achieved regarding both mechanically robust and high-performance EMI shielding MXene-based materials [20,21]. For example, conductive poly(3,4-ethylenedioxythiophene)-poly(styrenesulfonate) (PEDOT:PSS) was used to incorporate with $Ti_3C_2T_x$ to prepare composite film. The resulted $Ti_3C_2T_x$/PEDOT:PSS composite film exhibited a high EMI SE value of 42.10 dB and the tensile strength increased considerably from 5.62 to 13.71 MPa [20]. Cao et al. reported a MXene/cellulose nanofiber composite paper exhibiting an outstanding specific EMI shielding efficiency of 2647 dB·cm^2·g^{-1} (at 12.4 GHz, 90 wt% MXene content) with a tensile strength of about 44.3 MPa [21]. These polymers usually act as binders to improve the mechanical performance of composite film, however, the enhancement is not obvious due to their inherent low mechanical properties. Based on these problems, the aramid nanofiber (ANF) with high mechanical properties may be an alternative to incorporate with MXene for mechanically robust EMI shielding materials.

Kevlar is well-known as strong polymeric fibers with a tensile strength of ~3.6 GPa and modulus of ~90 GPa due to the high molecular orientation and strong interchain interactions [22–24]. After the pioneering work of Kotov's group on the preparation of ANF by feasible deprotonation of Kevlar macroscale fibers (KMF) [23], the ANF is believed to maintain good mechanical performance and has served as the building blocks for high-strength, flexible, and functional nanocomposite [25–29].

Here, we choose the ANF to integrate with MXene to optimize the mechanical properties of composite films featuring high EMI shielding performance. The ANF/MXene composite films are fabricated by simple vacuum-assisted filtration with a variety of MXene contents, and the associated mechanical and EMI shielding performances are tested. The highest electrical conductivity of 879.0 S/cm and EMI SE of 40.6 dB and SSE/t of 50491 dB·cm^2·g^{-1} with an ultrathin thickness of 3.2 μm were achieved at MXene content of 80 wt%. The ANF/MXene (60/40) composite film shows a mechanical strength of ~201.3 MPa, and also exhibits an excellent EMI shielding effectiveness (SE) of 28.1 dB with a thickness of 4.5 μm, which reveals the superiority of ANF/MXene composite film both in mechanical robustness and EMI shielding performance. In addition, our results may gain more insights in MXene/polymer composites for the design of high-performance EMI shielding materials with desired mechanical robustness.

2. Results and discussion

Fig. 1a shows a typical strategy for preparing few-layer MXene sheets through selectively etching of aluminum (Al) atoms of Ti_3AlC_2 (MAX) phase in a mixture of lithiumfluoride (LiF) and hydrochloric acid (HCl) [30]. The precursor, MAX, presents a dense, multilayered structure as shown in Fig. 1b. After the selectively etching process, the Al layer was removed, and a layered bulk Ti_3C_2 with an opening-book-like structure was formed in Fig. 1c. Through careful mechanical exfoliation via ultrasonation and repeatable shaking, the loosely layered Ti_3C_2 sheets turn into few-layer $Ti_3C_2T_x$ MXene sheets (T_x: surface-terminating functionality (e.g., F, O, and OH)), as shown in Fig. 1d, with the lateral size in the range of 0.4–5.2 μm. Fig. 1e shows the atomic force microscopy (AFM) image giving rise to the thickness of the few-layer MXene sheets in the range of 1.3–3.3 nm (Fig. S1). The transmission electron microscope (TEM) image in Fig. 1f indicates the clean surface of the MXene sheet, and the associated energy dispersive spectrometer

(EDS) elemental mapping images display the uniform distribution of Ti, C, O, and F elements, as shown in Fig. 1g. These features of 2D MXene sheets endow them with the capability of stacking together [17,20,21], integrating with other materials [31,32], as well as serving as fillers for functional composites [33–36].

As illustrated in Fig. 2a, the aramid nanofibers were prepared through a well-established deprotonation method [23]. During the preparation process, the interchain interactions between the molecular chains are weakened by the KOH-assisted deprotonation, which probably occurs by utilization of free hydrogen from -NH groups to increase electrostatic repulsion and subsequent reduction of the strength of hydrogen bonds between the molecular chains. Here, the Kevlar fibers possess an average diameter of about 12.4 ± 1.5 μm, as shown in Fig. 2b and S2. After the deprotonation process, the average diameter of obtained ANF decreases to around 11.9 ± 2.9 nm, and the length of ANF is about several micrometers, as shown in Fig. 2c, d, and S2.

The ANF/MXene composite films were fabricated through mixing MXene sheets and ANF suspensions together with a controllable weight ratio via a vacuum-assisted filtration process, as illustrated in Fig. 3a. Here, the thickness of the composite films would continually decrease from 6.0 ± 0.3 μm (pure ANF film) to 2.0 ± 0.1 μm (pure MXene film), as shown in Fig. 3b. Fig. S3 shows the the layered structural features of the as-prepared ANF/MXene composite films. Fig. 3c shows the characteristic (0 0 2) peak of composite films shifts from 6.7° to 5.4° after the introduction of ANF, which is due to the insertion of ANF and the separation of MXene sheets that affect the stacking of layered structure. As the intercalated ANF could expand the displacement between MXene nanosheets, the corresponding d-spacing of MXene sheets increases from approximately 13.2 Å (pure MXene film) to ~16.3 Å (ANF/MXene (90/10)). Furthermore, the microstructure of ANF/MXene film has been compared with the pure MXene and ANF films. In Fig. 3d, for the pure MXene film, the MXene sheets prefer to assemble and form layered structures, and the fractured surface features good orderliness. In contrast, the pure ANF film exhibits interconnect networks with hierarchical layered structure as shown in the morphologies of surface and cross-section. As expected, the ANF/MXene composite film presents an ordered lamellar structure, as verified from the morphologies of both surface and cross-section, consisted of alternately stacking of 2D MXene and one-dimensional (1D) ANF. Furthermore, the EDS elemental mapping images of ANF/MXene (60/40) exhibits a homogenous distribution of Ti in the composite papers (Fig. 3e), indicating a uniform distribution of MXene. The X-ray photoelectron spectroscopy (XPS) patterns of pure MXene and ANF/MXene (60/40) are presented in Fig. S4. The ratio of C/O atomic of the ANF/MXene was increased from 1.69 to 2.68 due to abundant C in ANF. Compared to MXene film, the C 1s spectrum of ANF/MXene (60/40) shows a new peak at 285.4 eV (C-N) and a stronger peak of C(O)O, indicating additional oxygen groups with introduction of ANF and resulting in more sites to form hydrogen bonds [37].

Fig. 4a shows typical tensile stress–strain curves of pure MXene film, ANF film, and ANF/MXene composite films. The pure MXene film shows a tensile strength of 43.2 ± 0.6 MPa and toughness of 0.5 ± 0.1 MJ/m^3 and exhibits poor mechanical performance. In comparison, the pure ANF film shows a tensile strength of 194.3 ± 10.3 MPa and toughness of 11.9 ± 1.3 MJ/m^3, which presents an excellent advantage in mechanical properties. As expected, after integrating with the ANF, significant enhancements in mechanical strength and toughness of the composite film have been verified, as summarized in Fig. 4b. Specifically, there is a continuous increase in both mechanical strength and toughness with an increasing ratio of ANF for ANF/MXene composite films. In detail, the mechanical strength can be above 200 MPa for ANF/MXene (60/40) and reach the highest strength of 232.0 ± 15.6 MPa (90/10), while the toughness can be improved up to 13.4 ± 2.3 MJ/m^3 (90/10).The Young's modulus of ANF/MXene composite films have also been summarized in Fig. S5. Compared with the pure MXene film (6.3 ± 0.7 GPa), the modulus of
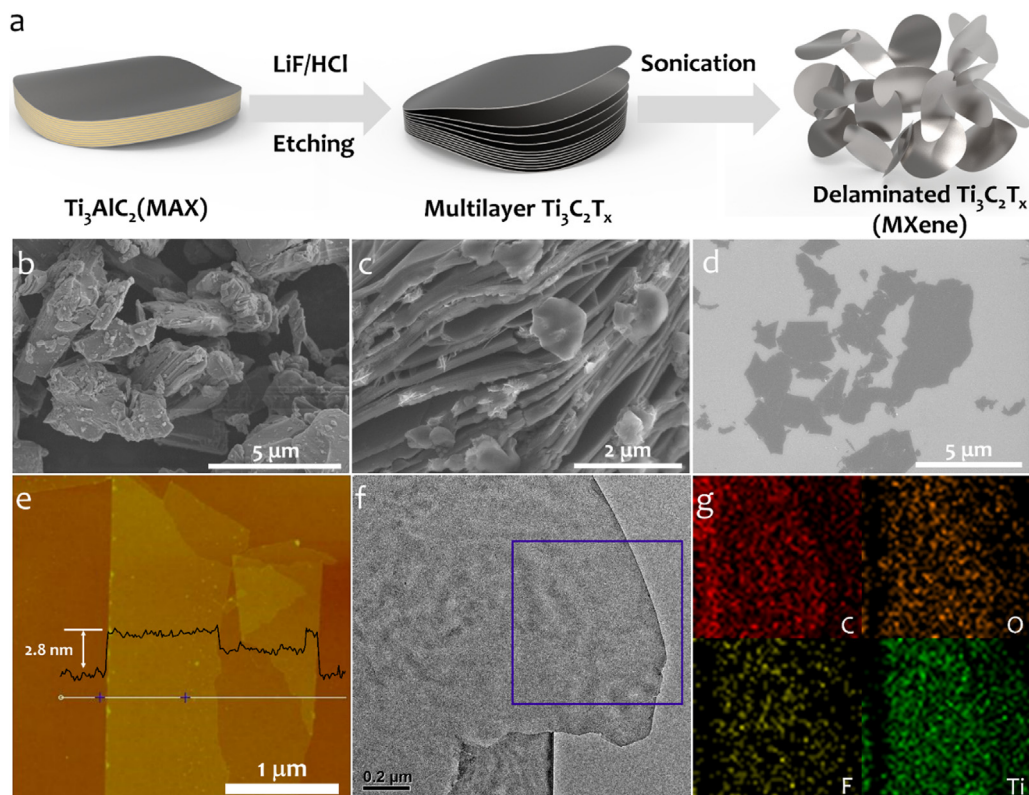
Fig. 1. Synthesis and characterization of MXene sheets. (a) Schematic illustration of the process of selectively etching for preparation of MXene. SEM images for (b) MAX, (c) multilayer MXene and (d) few-layer MXene, respectively. (e) AFM image of MXene sheet. (f) The TEM image and (g) corresponding EDS elemental mapping images of MXene. (For interpretation of the references to color in this figure legend, the reader is referred to the web version of this article.)
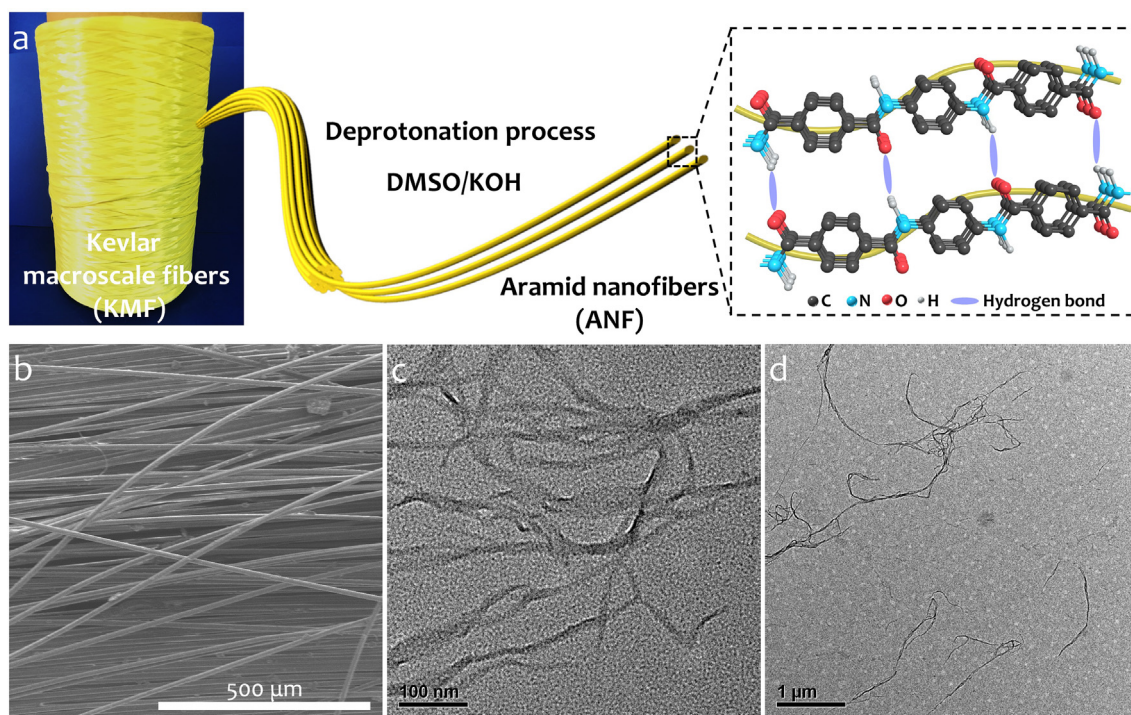

Fig. 2. (a) Schematic illustration of the preparation process for ANF. (b) SEM image for KMF. TEM images for (c) diameter and (d) length distribution of ANF. (For interpretation of the references to color in this figure legend, the reader is referred to the web version of this article.)

ANF/MXene (60/40) composite film has been improved to 13.8 ± 1.7 GPa. The increased modulus and strength for ANF/MXene composites indicate that the stress could be efficiently transferred between MXene and ANF due to the synergistic effect of the interlayer hydrogen bonding and intra-layer interaction [38,39]. As confirmed by Fourier transform infrared spectrometer (FTIR) in Fig. S6, wherein the peak at around 3434 cm^{-1} and 1643 cm^{-1} are assigned to the hydroxyl group and carbonyl group respectively. The rich hydroxyl groups on the surface of MXene and abundant carbonyl groups of ANF created favorable conditions to form hydrogen bonds [37,40]. Moreover, the increased intra-layer interaction also plays an important part in mechanical enhancement, as the large aspect ratio of ANF could easily intra-link the
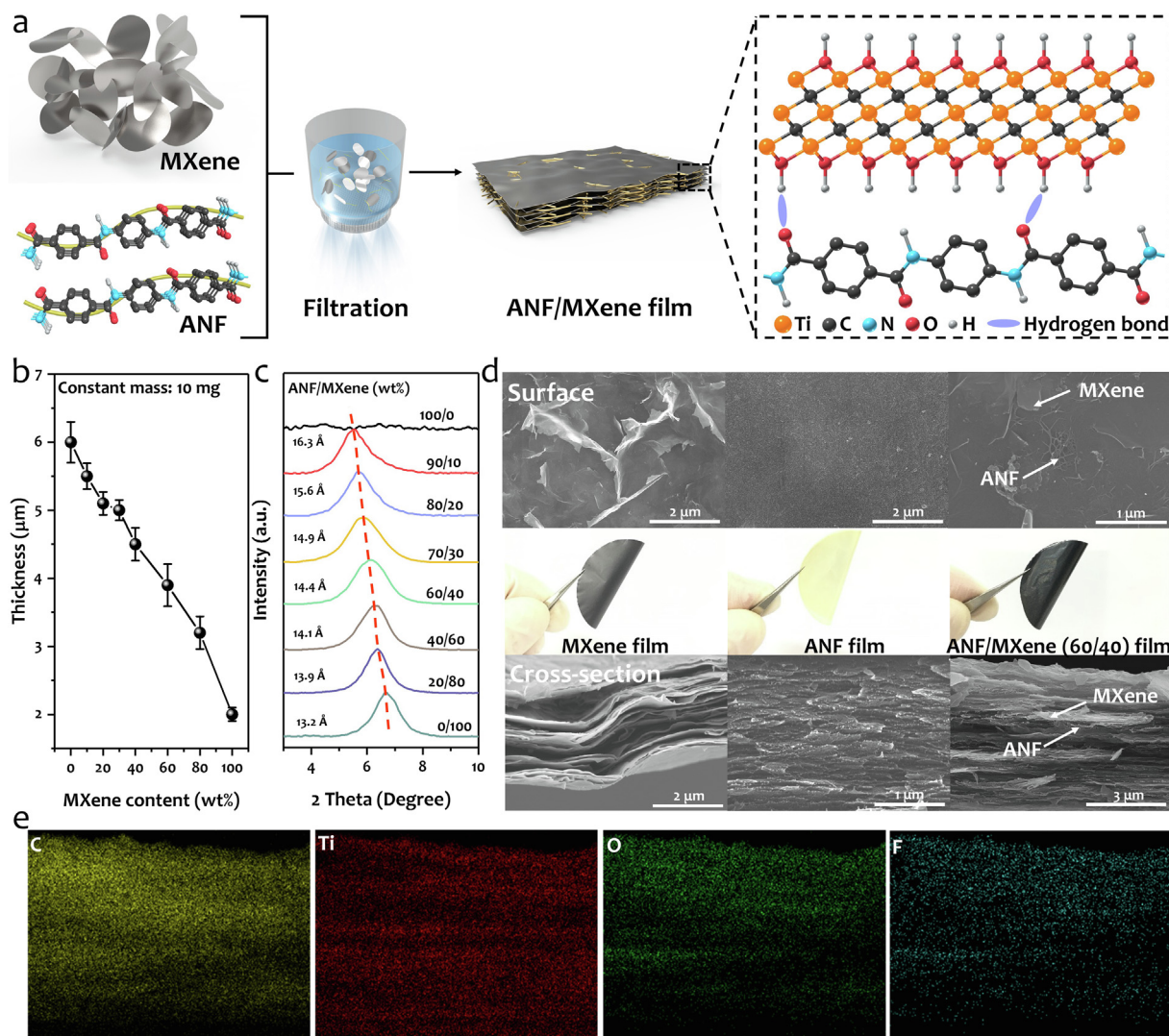
Fig. 3. (a) Illustration of the preparation process of the ANF/MXene composite film through filtration. (b) The thickness and (c) XRD patterns of ANF/MXene composite films with different ANF/MXene weight ratios. The ANF/MXene composite films were prepared with a constant mass of 10 mg. (d) Comparison of photographs and SEM images (surface and cross-section) among MXene, ANF and ANF/MXene (60/40) composite films. (e) The EDS mapping based on the SEM image of the cross-section of ANF/MXene (60/40) composite film in (d). (For interpretation of the references to color in this figure legend, the reader is referred to the web version of this article.)

nearby MXene nanosheets during the filtration process and eventually increased the stress transfer along the in-plane direction [39]. What's more, the interconnection networks of ANF and MXene nanosheets further increase the additional friction energy dissipation during the stretching process, which leads to an improvement in toughness [21]. In addition, different from our work, the ultrasonication treatment employed in recent works [41,42] may lead to the smaller size of MXene nanosheets and further deteriorate the mechanical performances of composites. Fig. 4c I-III show the flexibility of as-prepared ANF/MXene (60/40) composite films, where the sample was folded and unfolded without any damage. Furthermore, different from neat MXene film, the ANF/MXene (60/40) composite film maintains excellent structural integrity in respone to harsh sonication (in Fig. 4c IV and V), implying the relatively strong bonding interaction between ANF and MXene components.

The electrical conductivity of the ANF/MXene composite films is summarized in Fig. 5a. The conductivity of the pure MXene film is about 4515.0 S/cm, which is consistent with previous works [17,43]. As the MXene contents increase in the ANF/MXene composite films, the conductivity increases rapidly. The conductivity of the ANF/MXene composite film with 10 wt% MXene content can reach a value of 0.2 S/

cm, and the highest conductivity is about 879.0 S/cm when the MXene content is 80 wt%. Due to the high electrical conductivity of MXene, the pure MXene film shows a high EMI shielding effectiveness of 43.2 dB (2.0 μm), and the EMI SE would continually increase to 55.4 dB at a higher thickness of 6.0 μm. The pure ANF film presents almost zero in X-band as shown in Fig. S7. Compared with the pure MXene film, the EMI SE of ANF/MXene composite films is decreased due to the drop in electrical conductivity. Fig. 5b shows the corresponding EMI SE of ANF/MXene composite films in X-band (8.2–12.4 GHz). Specifically, the ANF/MXene (90/10) only shows an EMI SE of 5.2 dB. When the MXene contents increase to 30 wt%, the EMI SE would be larger than 20 dB, which was believed to qualify EMI shielding applications (above 20 dB) [44]. The highest EMI SE can be obtained as 40.6 dB with the MXene content of 80 wt%.

The EMI SE can be calculated by the Simon formalism for the highly conductive bulk materials [17,45,46]:

$$SE = 50 + 10\log(\frac{\sigma}{f}) + 1.7t(\sigma f)^{0.5}$$

where σ (S/cm) is the electrical conductivity, f (MHz) is the frequency, and t (cm) is the thickness of the composite film. The EMI SE strongly
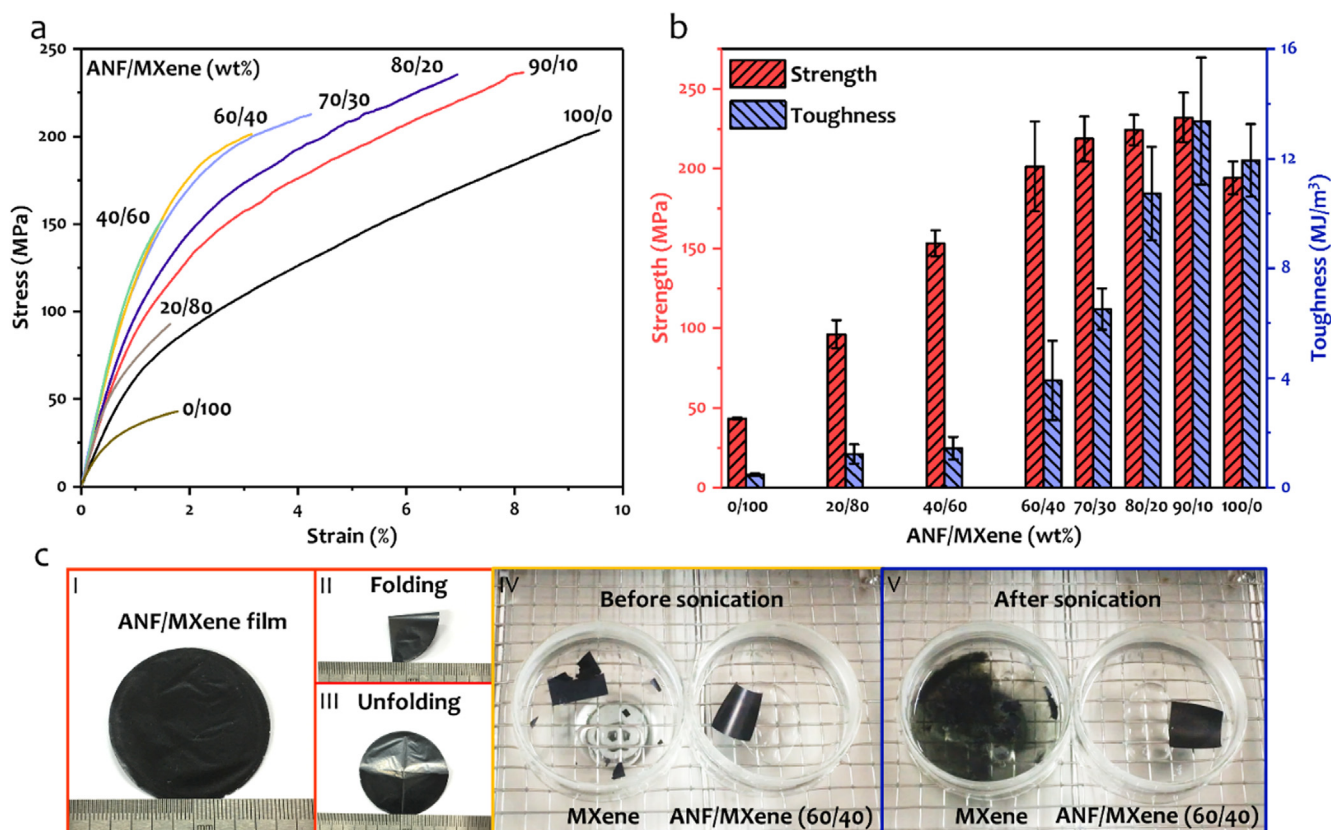
Fig. 4. (a) Typical tensile stress–strain curves of ANF/MXene composite films with different MXene contents. (b) Mechanical properties of ANF/MXene composite films (strength and toughness). (c) Digital image of the ANF/MXene composite film under different deformations. I: ANF/MXene (60/40) composite film; II, III: folding and unfolding; IV and V: the MXene and ANF/MXene films before and after sonication treatment. (For interpretation of the references to color in this figure legend, the reader is referred to the web version of this article.)

depends on the thickness and electrical conductivity of composite films. The experimental EMI SE data exhibit almost the same trend of the theoretical results (Fig. S8) and show comparable values at different MXene contents, as shown in Fig. 5c. In addition, considering the density and the thickness of the composite film, the specific SE (SSE/t, SE divided by the density and thickness) is usually calculated to evaluate the EMI effectiveness of composite films. As shown in Fig. S9, the SSE/t of the ANF/MXene composite films can reach a high value of 50491 dB·cm²·g⁻¹ with a MXene content of 80 wt%. Furthermore, the ANF/MXene (60/40) with a balance of the EMI shielding performance (28.1 dB) and mechanical strength (201.3 MPa) was chosen to prepare composite films with different thicknesses, as shown in Fig. S10. As expected, the EMI effectiveness would increase monotonically and reach a value of 44.7 dB when the thickness is 22.5 μm, as shown in Fig. 5d.

Furthermore, the possible propagation process of the electromagnetic waves have been speculated, as shown in Fig. 6a. When the incident electromagnetic waves contact the surface of the ANF/MXene composite film, a part of electromagnetic waves is reflected due to the impedance mismatch between air and composite film. The remaining electromagnetic waves enter the composite film and generate multiple reflection and absorption. The total EMI shielding effectiveness (SE_T) usually consists of the absorption of electromagnetic waves (SE_A), the reflection from materials (SE_R) and the multiple reflections in the internal of materials (SE_{MR}), while the SE_{MR} can be ignored when the SE_T is greater than 15 dB [20,47]. As shown in Fig. 6b, the SE_T, SE_A, and SE_R are calculated through the S parameters. The SE_T, SE_A, and SE_R would increase with the content of the MXene in ANF/MXene composite films, which is caused by the change of the conductivity of the composite film.

Interestingly, the SE_A is larger than the SE_R, thus, these EMI shielding materials are always suggested as absorption-dominant EMI shielding materials. However, it may be brutal to draw the conclusion according to the values of SE_A and SE_R, especially when the reflection takes place before absorption and most electromagnetic waves are reflected due to the impedance mismatch between free-space and composite film [48]. In addition, the absorption only exists in the rest of the electromagnetic waves that penetrate the composite film [48,49]. Accordingly, the corresponding power coefficients of reflectivity (R) and absorptivity (A) are calculated from the S parameters and then are employed to evaluate the interaction between electromagnetic waves and conductive composite films during the propagation process. As shown in Fig. 6c, the R increases as MXene content is enhanced, but the A displays an opposite trend. Specifically, the R increases from 0.22 to 0.97, and A decreases from 0.43 to 0.03, respectively, when MXene contents vary from 10 wt% to 80 wt%. For the qualified EMI shielding ANF/MXene composite films (SE > 20 dB), according to the power coefficients, we suggest that the ANF/MXene are reflection-dominant EMI shielding composite films.

To highlight the superior EMI shielding performance of ANF/MXene composite films with the consideration of the density and the thickness of EMI shielding materials in practical application, we employ the widely used SSE/t to compare the materials' EMI shielding performance. We summarized the SSE/t as a function of the thickness of different EMI shielding materials, such as carbon-based [50–58], metal-based [17,59] and MXene-based [17,20,21,41,42,60–65] EMI shielding materials in Fig. 7a. The detailed data about the comparison of SSE/t versus thickness are summarized in Table S1. Particularly, our ANF/MXene composite films exhibit comparable performance with high SSE/t (50491 dB·cm²·g⁻¹) and relatively low thickness (3.2 μm)
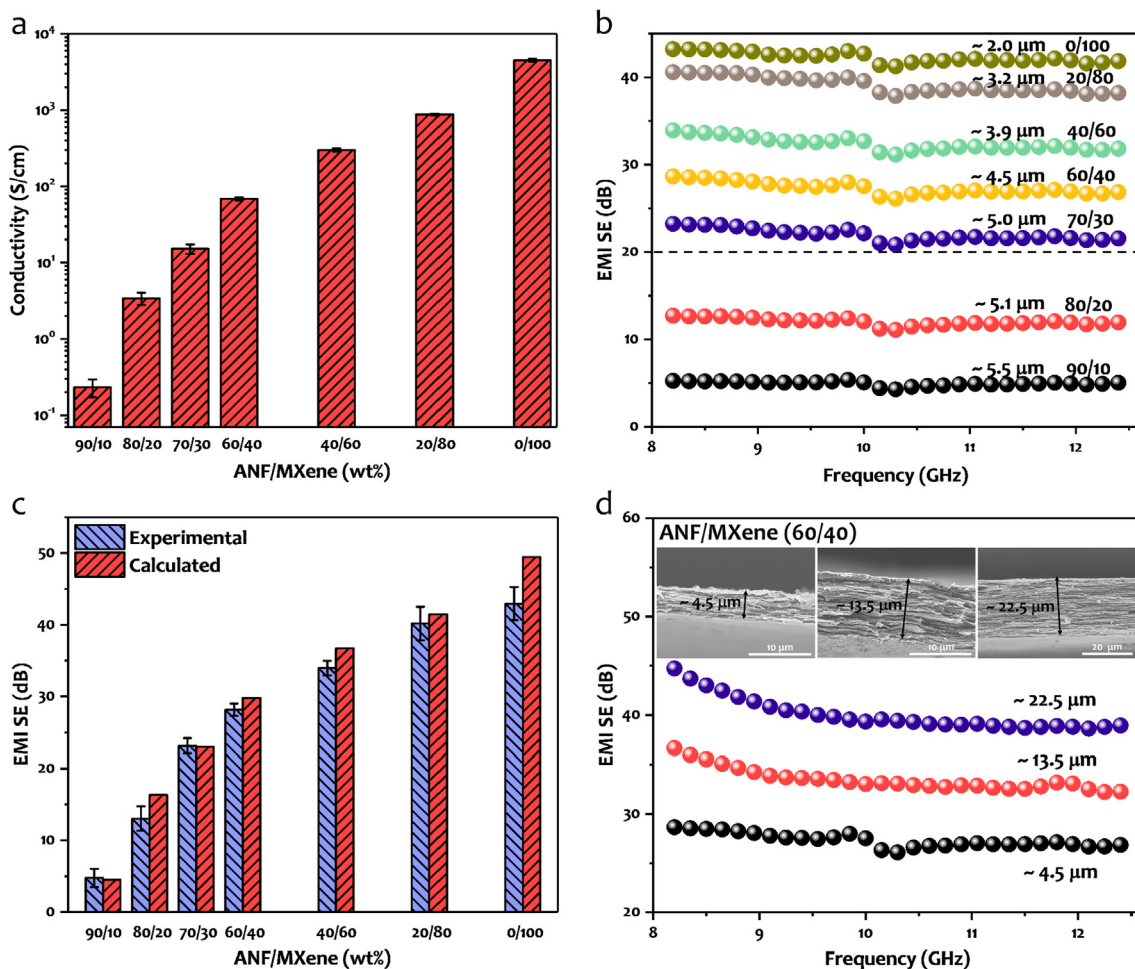
Fig. 5. (a) The conductivity and (b) EMI SE of ANF/MXene composite films. Dash line: common commercial EMI shielding requirement (above 20 dB). (c) The comparison between experimental and calculated EMI SE (at 8.2 GHz) of ANF/MXene composite films. (d) The EMI shielding effectiveness of ANF/MXene (60/40) with different thickness. Insets: the corresponding SEM images. (For interpretation of the references to color in this figure legend, the reader is referred to the web version of this article.)

according to the summary of previously reported EMI shielding materials. The layered microstructure also endows ANF/MXene composite films with high tensile strength, which is one of the important parameters for EMI shielding materials. To highlight the prominent advantage of ANF/MXene composite films, the comprehensive performance of ANF/MXene (60/40) and MXene films have been compared with other MXene-based composite films upon various parameters [20,21,60,64], including SSE/t, conductivity, thickness, strength, and toughness. As shown in Fig. 7b, a radar plot was drawn to compare with $Ti_3C_2T_x$/PEDOT:PSS [20], $Ti_3C_2T_x$/CNF [21], $Ti_3C_2T_x$/TOCNF [60] and MXene/MTM/PVA [64] composite film. The results are normalized by the maximum value of each parameter, and the detailed data are summarized in Table S2. Considering the comprehensive performance, the ANF/MXene composite film exhibits an excellent integration of SSE/t, conductivity, thickness, strength, and toughness, which is superior to the other four types of MXene-based composite films.

3. Conclusions

In conclusion, we have successfully fabricated an ultrathin, lightweight, and high mechanical strength ANF/MXene composite films with a layered microstructure and superior EMI shielding performance through a simple vacuum-assisted filtration process. Compared with the pure MXene film, the mechanical strength of the ANF/MXene composite films has been significantly improved to above 200 MPa (MXene content below 40 wt%). In addition, the ANF/MXene (20/80)

composite film exhibits an excellent EMI shielding performance of 40.6 dB and SSE/t of 50491 dB·cm^2·g^{-1} with an ultralow thickness of 3.2 μm. The balanced mechanical properties (201.3 MPa) and EMI shielding performance (28.1 dB) were achieved with 40 wt% MXene content. These performances guarantee the ultrathin and robust EMI shielding ANF/MXene composite films to satisfy various applications such as some highly integrated electronics (flexible and smart devices) and so on.

4. Experimental section

4.1. Materials

Kevlar 29 yarns were purchased from DuPont, USA. Dimethyl sulfoxide (DMSO) and Potassium hydroxide (KOH) were obtained from Beijing Chemical Works. Lithium fluoride (LiF, AR) was purchased from Aladdin Inc. (China). Ti_3AlC_2 powder (400 mesh) was purchased from Jilin 11 technology Co., Ltd.

4.2. Preparation of MXene

MXene was synthesis by selectively etching Al from the MAX phase (Ti_3AlC_2). In a typical etching method [30], 3.2 g LiF was dissolved in 40 ml of 9 M HCl in a Teflon container and further magnetically stirred 30 min. After that, 2 g Ti_3AlC_2 powder was gradually added, and the reaction was kept at 35 °C with continuous stirring for 24 h. Afterward,
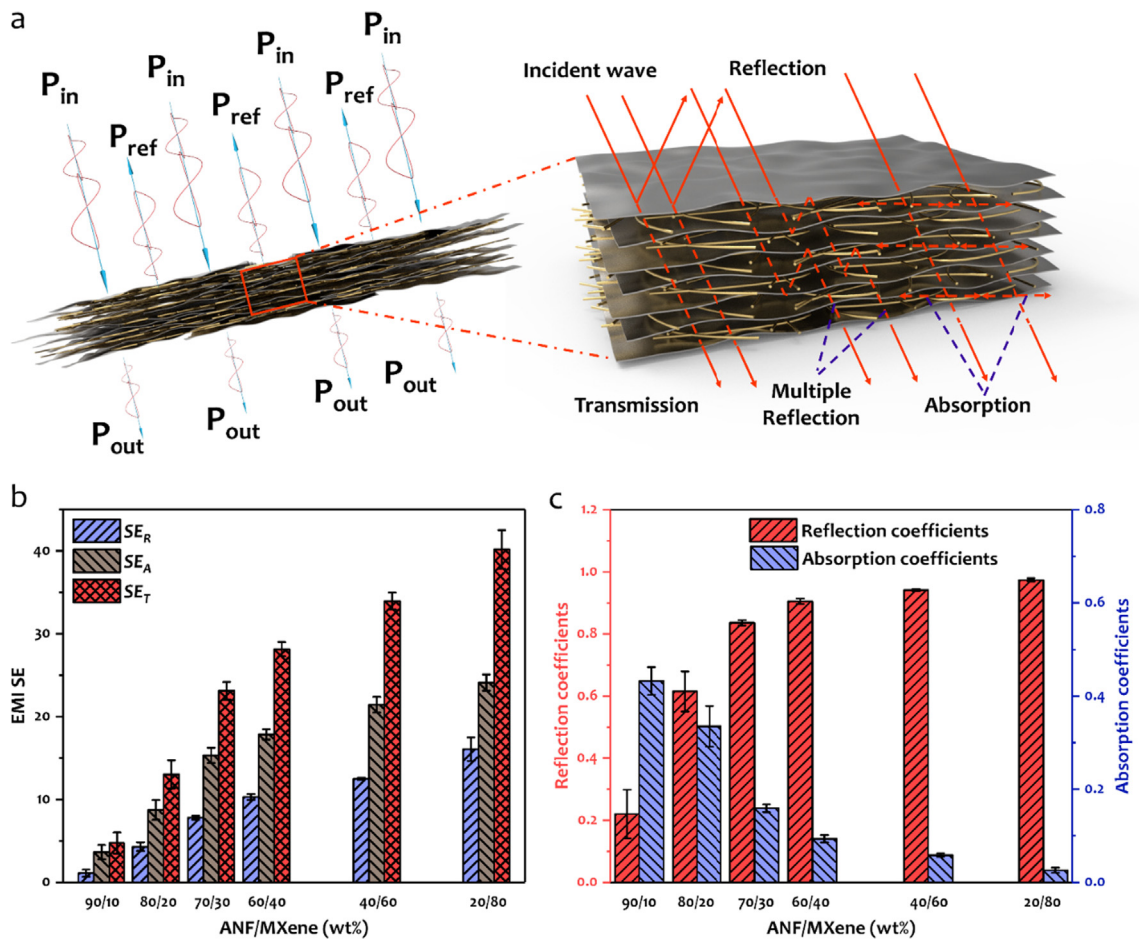
Fig. 6. (a) Schematic illustration for the explanation of the EMI shielding of ANF/MXene composite films. (b) Average EMI SE_T, SE_A, and SE_R and the corresponding (c) average power coefficients R and A value of ANF/MXene composite films. (For interpretation of the references to color in this figure legend, the reader is referred to the web version of this article.)

the obtained mixture solution was washed by H_2O with centrifugation and shaking until the pH of the dispersion was near neutral (3500 rpm, 5 min). Subsequently, the obtained sediment was dispersed in H_2O and bath sonicated for 30 min, followed by centrifugation for 1 h (3500 rpm). And the supernatant was collected for the preparation of composite films in this work.

4.3. Preparation of ANF

10.0 g of bulk Kevlar was dissolved in 1000 ml DMSO with 10.0 g KOH and further magnetically stirred for two weeks at room temperature to obtain ANF solution [23].
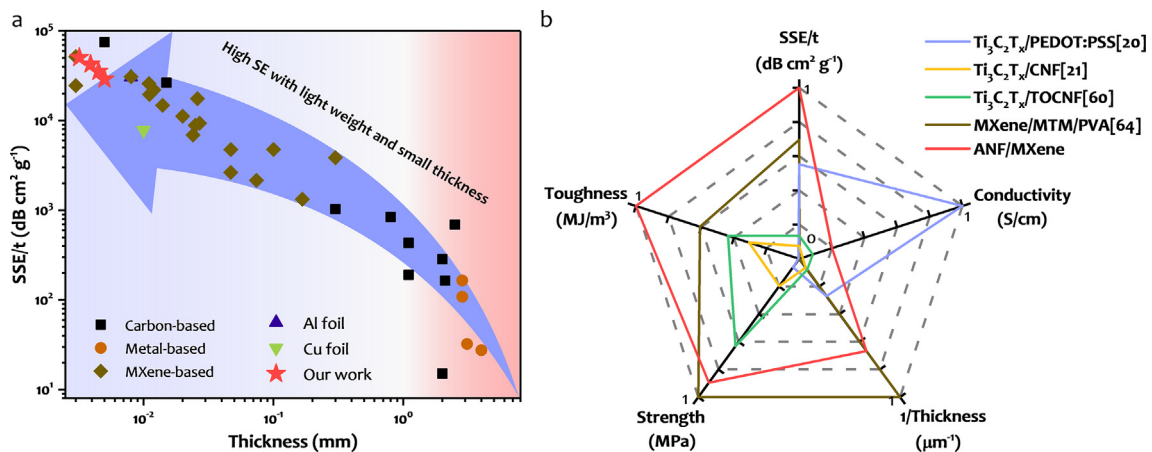

Fig. 7. (a) Comparison of the SSE/t as a function of the thickness of different EMI shielding materials. (b) A radar plot showing a comparison of comprehensive performance among $Ti_3C_2T_x$/PEDOT:PSS, $Ti_3C_2T_x$/CNF, $Ti_3C_2T_x$/TOCNF, MXene/MTM/PVA and ANF/MXene (60/40) composite films (PEDOT:PSS: poly(3,4-ethylenedioxythiophene) − poly(styrenesulfonate), PVA: polyvinyl alcohol, CNF: cellulose nanofiber, TOCNF: 2,2,6,6-tetramethyl-1-piperidinyloxy oxidized cellulose nanofiber, MTM: montmorillonite). (For interpretation of the references to color in this figure legend, the reader is referred to the web version of this article.)

4.4. Preparation of MXene film and ANF/MXene composite films

MXene solution was dispersed in deionized water (0.5 mg/ml), and the MXene film was prepared through a simple vacuum-assisted filtration method by a mix cellulose membrane filter (0.22 μm pore size), following drying in oven and peeling off from the filter. The ANF solution was mixed with water and stirred to homogenous dispersion (0.5 mg/ml). Then the MXene suspension was mixed with ANF solution by a Planetary Vacuum Mixer (THINKY ARV-310), and a series of ANF/MXene solution with different MXene contents (90/10, 80/20, 70/30, 60/40, 40/60, and 20/80) were prepared. The mixed solution was filtrated by a PTFE membrane (0.22 μm pore size) and dried in an oven to prepare the composite films. Then, the ANF/MXene composite films were immersed in water for 24 h to remove the KOH.

4.5. Characterization

The morphologies of MAX powder, MXene sheets, and ANF/MXene composite films were examined by scanning electron microscope (SEM, Hitachi S4800). The diameter of ANF was measured by a field emission transmission electron microscope (TEM, Tecnai G2 F20 U-TWIN). The thickness of the MXene sheet was measured by atomic force microscopy (AFM, Dimension Icon Bruker). X-ray diffraction (XRD) patterns of MXene film and ANF/MXene composite films were measured by a Rigaku SmartLab 9 kW XRD (Cu Kα radiation, 40.0 Kv, and 200.0 mA) with a scan speed of 10.0 degrees per minute. Elemental compositions of sample were conducted by X-ray photoelectron spectroscopy (ESCALAB250Xi, Thermo Scientific). FTIR spectroscopy was obtained using a FTIR spectrometer (Spectrum One, Perkin Elmer Instruments). The mechanical properties of MXene film, ANF film, and ANF/MXene composite films were measured by a dynamic thermomechanical analysis (DMA Q800, TA), the films were cut into strips ($20 \times 2 \text{ mm}^2$) before the tensile test, and more than five samples of different MXene contents were prepared for tensile test. The resistance of MXene film and ANF/MXene composite films were measured by a High-performance multimeter (KEITHLEY, DMM 7510).

4.6. Electromagnetic shielding effectiveness

EMI SE characterization was measured through the waveguide method by using a vector network analyzer (Agilent E8363B PNA-L) in the frequency range of 8.2–12.4 GHz (X-band). Scotch tape was attached to the round of the film to mount it onto the sample holder, and more than four samples were prepared for EMI testing. According to the possible mechanism of the composite film, the incident power (P_{in}), reflected power (P_{ref}) and remaining power (P_{out}) were used to calculate the EMI SE combined with the S parameters, as shown in the following formulas.

$$R = |S_{11}|^2 \quad T = |S_{21}|^2 \quad A + T + R = 1$$

$$SE_T (dB) = 10\log\frac{P_{in}}{P_{out}} = 10\log\frac{1}{|S_{21}|^2}$$

$$SE_R (dB) = 10\log\frac{P_{in}}{P_{in} - P_{ref}} = 10\log\frac{1}{1 - |S_{11}|^2}$$

$$SE_A (dB) = SE_T - SE_R$$

where R, T, and A are the reflection, transmission, and absorption coefficients, respectively. SE_T, SE_R, and SE_A are the total, reflective, and absorptive EMI SE, respectively.

CRediT authorship contribution statement

Chuanxin Weng: Conceptualization, Methodology, Investigation, Visualization, Writing - original draft. **Tianle Xing:** Validation, Investigation. **Hao Jin:** Writing - review & editing. **Guorui Wang:** Writing - review & editing. **Zhaohe Dai:** Writing - review & editing. **Yongmao Pei:** Investigation. **Luqi Liu:** Conceptualization, Visualization, Writing - review & editing. **Zhong Zhang:** Supervision, Project administration.

Conflicts of interest

There are no conflicts to declare.

Appendix A. Supplementary material

Supplementary data to this article can be found online at https://doi.org/10.1016/j.compositesa.2020.105927.

References

[1] Zeng ZH, Chen MJ, Jin H, Li WW, Xue X, Zhou LC, et al. Thin and flexible multi-walled carbon nanotube/waterborne polyurethane composites with high-performance electromagnetic interference shielding. Carbon 2016;96:768–77.

[2] Xia Q, Zhang Z, Chu H, Liu Y, Leng J. Research on high electromagnetic interference shielding effectiveness of a foldable buckypaper/polyacrylonitrile composite film via interface reinforcing. Compos Part A 2018;113:132–40.

[3] Li H, Yuan D, Li P, He C. High conductive and mechanical robust carbon nanotubes/waterborne polyurethane composite films for efficient electromagnetic interference shielding. Compos Part A 2019;121:411–7.

[4] Song W-L, Cao M-S, Lu M-M, Bi S, Wang C-Y, Liu J, et al. Flexible graphene/polymer composite films in sandwich structures for effective electromagnetic interference shielding. Carbon 2014;66:67–76.

[5] Chen J, Xu J, Wang K, Qian X, Sun R. Highly thermostable, flexible, and conductive films prepared from cellulose, graphite, and polypyrrole nanoparticles. ACS Appl Mater Interfaces 2015;7(28):15641–8.

[6] Jia L-C, Sun W-J, Zhou C-G, Yan D-X, Zhang Q-C, Li Z-M. Integrated strength and toughness in graphene/calcium alginate films for highly efficient electromagnetic interference shielding. J Mater Chem C 2018;6(34):9166–74.

[7] Al-Saleh MH, Gelves GA, Sundararaj U. Copper nanowire/polystyrene nanocomposites: lower percolation threshold and higher EMI shielding. Compos Part A 2011;42(1):92–7.

[8] Jung J, Lee H, Ha I, Cho H, Kim KK, Kwon J, et al. Highly stretchable and transparent electromagnetic interference shielding film based on silver nanowire percolation network for wearable electronics applications. ACS Appl Mater Interfaces 2017;9(51):44609–16.

[9] Kim DG, Choi JH, Choi DK, Kim SW. Highly bendable and durable transparent electromagnetic interference shielding film prepared by wet sintering of silver nanowires. ACS Appl Mater Interfaces 2018;10(35):29730–40.

[10] Li J, Peng W-J, Fu Z-J, Tang X-H, Wu H, Guo S, et al. Achieving high electrical conductivity and excellent electromagnetic interference shielding in poly(lactic acid)/silver nanocomposites by constructing large-area silver nanoplates in polymer matrix. Compos B 2019;171:204–13.

[11] Tan Y-J, Li J, Cai J-H, Tang X-H, Liu J-H, Hu Z-q, et al. Comparative study on solid and hollow glass microspheres for enhanced electromagnetic interference shielding in polydimethylsiloxane/multi-walled carbon nanotube composites. Compos B 2019;177:107378.

[12] Li J, Chen JL, Tang XH, Cai JH, Liu JH, Wang M. Constructing nanopores in poly (oxymethylene)/multi-wall carbon nanotube nanocomposites via poly(l-lactide) assisting for improving electromagnetic interference shielding. J Colloid Interface Sci 2020;565:536–45.

[13] Tang X-H, Li J, Tan Y-J, Cai J-H, Liu J-H, Wang M. Achieve high performance microwave shielding in poly(ε-caprolactone)/multi-wall carbon nanotube composites via balancing absorption in conductive domains and multiple scattering at interfaces. Appl Surf Sci 2020;508:145178.

[14] Naguib M, Kurtoglu M, Presser V, Lu J, Niu J, Heon M, et al. Two-dimensional nanocrystals produced by exfoliation of Ti₃AlC₂. Adv Mater 2011;23(37):4248–53.

[15] Lipatov A, Alhabeb M, Lukatskaya MR, Boson A, Gogotsi Y, Sinitskii A. Effect of synthesis on quality, electronic properties and environmental stability of individual monolayer Ti₃C₂ MXene flakes. Adv Electron Mater 2016;2(12):1600255.

[16] Gogotsi Y, Anasori B. The rise of MXenes. ACS Nano 2019;13(8):8491–4.

[17] Shahzad F, Alhabeb M, Hatter CB, Anasori B, Man Hong S, Koo CM, et al. Electromagnetic interference shielding with 2D transition metal carbides (MXenes). Science 2016;353(6304):1137–40.

[18] Liu J, Zhang HB, Sun R, Liu Y, Liu Z, Zhou A, et al. Hydrophobic, flexible, and lightweight MXene foams for high-performance electromagnetic-interference shielding. Adv Mater 2017;29(38):1702367.

[19] Weng C, Wang G, Dai Z, Pei Y, Liu L, Zhang Z. Buckled AgNW/MXene hybrid hierarchical sponges for high-performance electromagnetic interference shielding. Nanoscale 2019;11(47):22804–12.

[20] Liu R, Miao M, Li Y, Zhang J, Cao S, Feng X. Ultrathin biomimetic polymeric Ti$_3$C$_2$T$_x$ MXene composite films for electromagnetic interference shielding. ACS Appl Mater Interfaces 2018;10(51):44787–95.

[21] Cao WT, Chen FF, Zhu YJ, Zhang YG, Jiang YY, Ma MG, et al. Binary strengthening and toughening of MXene/cellulose nanofiber composite paper with nacre-inspired structure and superior electromagnetic interference shielding properties. ACS Nano 2018;12(5):4583–93.

[22] Vollrath F, Knight DP. Liquid crystalline spinning of spider silk. Nature 2001;410:541.

[23] Yang M, Cao K, Sui L, Qi Y, Zhu J, Waas A, et al. Dispersions of aramid nanofibers: a new nanoscale building block. ACS Nano 2011;5(9):6945–54.

[24] Kwon SR, Harris J, Zhou T, Loufakis D, Boyd JG, Lutkenhaus JL. Mechanically strong graphene/aramid nanofiber composite electrodes for structural energy and power. ACS Nano 2017;11(7):6682–90.

[25] Cao K, Siepermann CP, Yang M, Waas AM, Kotov NA, Thouless MD, et al. Reactive aramid nanostructures as high-performance polymeric building blocks for advanced composites. Adv Funct Mater 2013;23(16):2072–80.

[26] Tung SO, Ho S, Yang M, Zhang R, Kotov NA. A dendrite-suppressing composite ion conductor from aramid nanofibres. Nat Commun 2015;6:6152.

[27] Lyu J, Wang X, Liu L, Kim Y, Tanyi EK, Chi H, et al. High strength conductive composites with plasmonic nanoparticles aligned on aramid nanofibers. Adv Funct Mater 2016;26(46):8435–45.

[28] Lyu J, Zhao X, Hou X, Zhang Y, Li T, Yan Y. Electromagnetic interference shielding based on a high strength polyaniline-aramid nanocomposite. Compos Sci Technol 2017;149:159–65.

[29] Lyu J, Liu Z, Wu X, Li G, Fang D, Zhang X. Nanofibrous Kevlar aerogel films and their phase-change composites for highly efficient infrared stealth. ACS Nano 2019;13(2):2236–45.

[30] Alhabeb M, Maleski K, Anasori B, Lelyukh P, Clark L, Sin S, et al. Guidelines for synthesis and processing of two-dimensional titanium carbide (Ti$_3$C$_2$T$_x$ MXene). Chem Mater 2017;29(18):7633–44.

[31] Zhao MQ, Ren CE, Ling Z, Lukatskaya MR, Zhang C, Van Aken KL, et al. Flexible MXene/carbon nanotube composite paper with high volumetric capacitance. Adv Mater 2015;27(2):339–45.

[32] Yan J, Ren CE, Maleski K, Hatter CB, Anasori B, Urbankowski P, et al. Flexible MXene/graphene films for ultrafast supercapacitors with outstanding volumetric capacitance. Adv Funct Mater 2017;27(30).

[33] Sun RH, Zhang HB, Liu J, Xie X, Yang R, Li Y, et al. Highly conductive transition metal carbide/carbonitride(MXene)@polystyrene nanocomposites fabricated by electrostatic assembly for highly efficient electromagnetic interference shielding. Adv Funct Mater 2017;27(45):1702807.

[34] Wang L, Chen L, Song P, Liang C, Lu Y, Qiu H, et al. Fabrication on the annealed Ti$_3$C$_2$T$_x$ MXene/epoxy nanocomposites for electromagnetic interference shielding application. Compos B 2019;171:111–8.

[35] Rajavel K, Luo S, Wan Y, Yu X, Hu Y, Zhu P, et al. 2D Ti$_3$C$_2$T$_x$ MXene/poly-vinylidene fluoride (PVDF) nanocomposites for attenuation of electromagnetic radiation with excellent heat dissipation. Compos A 2020;129:105693.

[36] Zhao S, Zhang HB, Luo JQ, Wang QW, Xu B, Hong S, et al. Highly electrically conductive three-dimensional Ti$_3$C$_2$T$_x$ MXene/reduced graphene oxide hybrid aerogels with excellent electromagnetic interference shielding performances. ACS Nano 2018;12(11):11193–202.

[37] Zhang Z, Yang S, Zhang P, Zhang J, Chen G, Feng X. Mechanically strong MXene/Kevlar nanofiber composite membranes as high-performance nanofluidic osmotic power generators. Nat Commun 2019;10(1):2920.

[38] Ling Z, Ren CE, Zhao MQ, Yang J, Giammarco JM, Qiu J, et al. Flexible and conductive MXene films and nanocomposites with high capacitance. Proc Natl Acad Sci USA 2014;111(47):16676–81.

[39] Liu Q, Liu L, Kuang J, Dai Z, Han J, Zhang Z. Nanostructured carbon materials based electrothermal air pump actuators. Nanoscale. 2014;6(12):6932–8.

[40] Kwon SR, Elinski MB, Batteas JD, Lutkenhaus JL. Robust and flexible aramid nanofiber/graphene layer-by-layer electrodes. ACS Appl Mater Interfaces 2017;9(20):17125–35.

[41] Xie F, Jia F, Zhuo L, Lu Z, Si L, Huang J, et al. Ultrathin MXene/aramid nanofiber composite paper with excellent mechanical properties for efficient electromagnetic interference shielding. Nanoscale 2019;11(48):23382–91.

[42] Wei H, Wang M, Zheng W, Jiang Z, Huang Y. 2D Ti$_3$C$_2$T$_x$ MXene/aramid nanofibers composite films prepared via a simple filtration method with excellent mechanical and electromagnetic interference shielding properties. Ceram Int 2020;46(5):6199–204.

[43] Dillon AD, Ghidiu MJ, Krick AL, Griggs J, May SJ, Gogotsi Y, et al. Highly conductive optical quality solution-processed films of 2D titanium carbide. Adv Funct Mater 2016;26(23):4162–8.

[44] Wang SJ, Li DS, Jiang L. Synergistic effects between MXenes and Ni chains in flexible and ultrathin electromagnetic interference shielding films. Adv Mater Interfaces. 2019;6(19):1900961.

[45] Simon RM. EMI shielding through conductive plastics. Polym-Plast Technol Eng 1981;17(1):1–10.

[46] Das NC, Liu Y, Yang K, Peng W, Maiti S, Wang H. Single-walled carbon nanotube/poly(methyl methacrylate) composites for electromagnetic interference shielding. Polym Eng Sci 2009;49(8):1627–34.

[47] Chen Z, Xu C, Ma C, Ren W, Cheng HM. Lightweight and flexible graphene foam composites for high-performance electromagnetic interference shielding. Adv Mater 2013;25(9):1296–300.

[48] Song Q, Ye F, Yin X, Li W, Li H, Liu Y, et al. Carbon nanotube-multilayered graphene edge plane core-shell hybrid foams for ultrahigh-performance electromagnetic-interference shielding. Adv Mater 2017;29(31):1701583.

[49] Wan YJ, Zhu PL, Yu SH, Sun R, Wong CP, Liao WH. Anticorrosive, ultralight, and flexible carbon-wrapped metallic nanowire hybrid sponges for highly efficient electromagnetic interference shielding. Small 2018;14(27):1800534.

[50] Yan D-X, Pang H, Li B, Vajtai R, Xu L, Ren P-G, et al. Structured reduced graphene oxide/polymer composites for ultra-efficient electromagnetic interference shielding. Adv. Funct Mater 2015;25(4):559–66.

[51] Song W-L, Guan X-T, Fan L-Z, Cao W-Q, Wang C-Y, Zhao Q-L, et al. Magnetic and conductive graphene papers toward thin layers of effective electromagnetic shielding. J Mater Chem A 2015;3(5):2097–107.

[52] Agnihotri N, Chakrabarti K, De A. Highly efficient electromagnetic interference shielding using graphite nanoplatelet/poly(3,4-ethylenedioxythiophene)–poly(styrenesulfonate) composites with enhanced thermal conductivity. RSC Adv 2015;5(54):43765–71.

[53] Pande S, Chaudhary A, Patel D, Singh BP, Mathur RB. Mechanical and electrical properties of multiwall carbon nanotube/polycarbonate composites for electrostatic discharge and electromagnetic interference shielding applications. RSC Adv 2014;4(27):13839–49.

[54] Al-Saleh MH, Saadeh WH, Sundararaj U. EMI shielding effectiveness of carbon based nanostructured polymeric materials: a comparative study. Carbon 2013;60:146–56.

[55] Arjmand M, Apperley T, Okoniewski M, Sundararaj U. Comparative study of electromagnetic interference shielding properties of injection molded versus compression molded multi-walled carbon nanotube/polystyrene composites. Carbon 2012;50(14):5126–34.

[56] Ghosh P, Chakrabarti A. Conducting carbon black filled EPDM vulcanizates: assessment of dependence of physical and mechanical properties and conducting character on variation of filler loading. Eur Polym J 2000;36(5):1043–54.

[57] Zhou E, Xi J, Guo Y, Liu Y, Xu Z, Peng L, et al. Synergistic effect of graphene and carbon nanotube for high-performance electromagnetic interference shielding films. Carbon 2018;133:316–22.

[58] Li H, Lu X, Yuan D, Sun J, Erden F, Wang F, et al. Lightweight flexible carbon nanotube/polyaniline films with outstanding EMI shielding properties. J Mater Chem C 2017;5(34):8694–8.

[59] Shui X, Chung DDL. Nickel filament polymer-matrix composites with low surface impedance and high electromagnetic interference shielding effectiveness. J Electron Mater 1997;26(8):928–34.

[60] Zhan ZY, Song QC, Zhou ZH, Lu CH. Ultrastrong and conductive MXene/cellulose nanofiber films enhanced by hierarchical nano-architecture and interfacial interaction for flexible electromagnetic interference shielding. J Mater Chem C 2019;7(32):9820–9.

[61] Xu H, Yin X, Li X, Li M, Liang S, Zhang L, et al. Lightweight Ti$_2$CT$_x$ MXene/poly(vinyl alcohol) composite foams for electromagnetic wave shielding with absorption-dominated feature. ACS Appl Mater Interfaces 2019;11(10):10198–207.

[62] Jin XX, Wang JF, Dai LZ, Liu XY, Li L, Yang YY, et al. Flame-retardant poly(vinyl alcohol)/MXene multilayered films with outstanding electromagnetic interference shielding and thermal conductive performances. Chem Eng J 2020;380:122475.

[63] Zhou Z, Liu J, Zhang X, Tian D, Zhan Z, Lu C. Ultrathin MXene/calcium alginate aerogel film for high-performance electromagnetic interference shielding. Adv Mater Interfaces. 2019;6(6):1802040.

[64] Lipton J, Weng GM, Alhabeb M, Maleski K, Antonio F, Kong J, et al. Mechanically strong and electrically conductive multilayer MXene nanocomposites. Nanoscale 2019;11(42):20295–300.

[65] Chen H, Wen Y, Qi Y, Zhao Q, Qu L, Li C. Pristine titanium carbide MXene films with environmentally stable conductivity and superior mechanical strength. Adv Funct Mater 2020;30(5):1906996.